



OPEN

# The exact analytical solution of the dual-phase-lag two-temperature bioheat transfer of a skin tissue subjected to constant heat flux

Hamdy M. Youssef<sup>1</sup>✉ & Najat A. Alghamdi<sup>2</sup>

This work is dealing with the temperature reaction and response of skin tissue due to constant surface heat flux. The exact analytical solution has been obtained for the two-temperature dual-phase-lag (TTDPL) of bioheat transfer. We assumed that the skin tissue is subjected to a constant heat flux on the bounding plane of the skin surface. The separation of variables for the governing equations as a finite domain is employed. The transition temperature responses have been obtained and discussed. The results represent that the dual-phase-lag time parameter, heat flux value, and two-temperature parameter have significant effects on the dynamical and conductive temperature increment of the skin tissue. The Two-temperature dual-phase-lag (TTDPL) bioheat transfer model is a successful model to describe the behavior of the thermal wave through the skin tissue.

The thermal transfer through a living skin tissue is extremely essential to a wide range of therapies and their applications<sup>1</sup>. Improvements in the microwave, laser, and other technologies also extended bioheat transfer work. Several researchers comment on biothermal transmission analyzes in biological living tissues, including Pennes<sup>2</sup>. He optimized the parabolic model for biological tissues for the first bioheat transfer. Also, the Pennes biological transmission method is used to model the nature and consistency of thermal behavior in biological tissues and living bodies. External similarities to such unpredictable results that display non-Fourier or hyperbolic conduction behavior. Cattaneo<sup>3</sup> and Vernotte<sup>4</sup> provided different modulations of Fourier's law of heat conduction as a linear extension form of the Fourier law to describe the hyperbolic equation type. They suggested a model of thermal waves measure the effect of microwave and thermal flux activity. Different forms of work have been undertaken to address various skin tissue conditions without damaging the balanced tissue surrounding them. Xu et al.<sup>5</sup> solved analytical the Pennes bioheat transfer equation (PBTE), reviewed skin bioheat transfer, skin structure, thermal damage, skin biomechanics, and bio-thermomechanics. The non-Fourier thermomechanical activity of skin tissues under various surface thermal loading limits was analyzed in DPL, hyperbolic and parabolic models of biomass transport, Xu and al. studied and noticed substantial variations between Pennes, thermal wave and DPL anticipations models<sup>6</sup>. Also, Rossmann et al.<sup>7</sup> reviewed the temperature dependence of the dielectric properties, thermal properties, and perfusion of biological tissues at hyper-thermic and ablation temperatures. Poor et al.<sup>8</sup> focused on the temperature disturbance of skin tissue due to time-dependent surface heating. Tzou's model has been extended by the dual-phase-lag principle, with the delayed activity in a high rate of response taken into consideration. Although the process is lagging, the small-scale response is caught in time<sup>9,10</sup>. Tzou<sup>11</sup> introduced a phase-lag for a temperature gradient. Askarizadeh et al.<sup>12</sup> utilized the dual-phase-lag (DPL) model in treating the transient heat transfer problems in skin tissue. Dutta and Kundu established a two-dimensional thermal model of malignant tissues, focused on the bi-dimensional local thermal non-balance therapy model for bio-heat<sup>13</sup>.

<sup>1</sup>Mechanical Engineering Department, College of Engineering and Islamic Architecture, Umm Al-Qura University, Mecca, Saudi Arabia. <sup>2</sup>Department of Mathematics, Faculty of Applied Science, Umm Al-Qura University, Mecca, Saudi Arabia. ✉email: [youssefanne2005@gmail.com](mailto:youssefanne2005@gmail.com)

Liu et al. first address the overall bioheat transmission paradigm in living tissue and analyze<sup>14</sup>. Liu et al. are tested during the hyperthermia procedure in the two-stage model for heat transfer problems in the biological tissue<sup>15,16</sup>. The Liu and Chen thermal conductor model (DPL) used the non-Fourier thermal activity for the diagnosis of hyperthermia to describe the thermal transportation occurring in biological tissue<sup>17</sup>. In terms of the properties of blood and tissue and the interphase charge of the heat transfer parameter and perfusion rate, Zhang articulated phase lag or relaxation periods<sup>18</sup>. He observed that the lag periods are very similar together for living tissues. Dutta and Kundu performed a thermal wave propagation study for a constant and variable flux of heat on a skin tissue surface in biological tissue, connected with the diagnosis of hyperthermia.<sup>19</sup>

A finite element approach to the temperature distribution of deep skin tissues in the human limb was suggested by Agrawal et al.<sup>20</sup>. Kumar et al. also researched the thermal behavior, using a dual-phase-lag (DPL) model of time-fractional<sup>21</sup>. To address the effect of injecting nanoparticles in irregularly-shaped liver tumors on cancer cells, Shao et al. have developed an RFA model<sup>22</sup>. A dual-phase-lag (DPL) bioheat transfer model analysis approach was used by Poor et al. on the skin tissue as the finite domain of continuous, cosine, and pulse heat flow conditions on the surface of the skin<sup>8</sup>.

Liu and Xu developed a closed-form analytical approach for the Pennes bioheat equation solution for changes in skin tissue temperature induced by sinusoidal heat flow<sup>23</sup>. Shih et al. have overcome the consequence of a semi-infinite biological skin tissue temperature reaction study undergoing sine flux<sup>24</sup>. Regarding periodic constant and pulsed train heat flux boundary conditions, Ahmadika et al. shall have the analytical solution for the bioheat (parabolize) and hyperbolized bioheat transfer models of the Penne<sup>25</sup>. The statistical model was used by Horng et al. to explain the effects of pulsatile blood flow in the thermal disruption<sup>26</sup>. He found out that the influence on the thermal area on tumor and the slight variation only on a blood continuum range from standard to parabolic, velocity profiles on the blood flow. Shih et al. investigated the coupled effects of the pulsatile blood flow and thermal relaxation time in living tissues during thermal treatments<sup>27</sup>. Youssef and Alghamdi<sup>28</sup> have solved a one-dimensional application of thermoelastic dual-phase-lag skin tissue under specific thermal loading. Kundu and Dewanjee<sup>29</sup> introduced a new method for non-Fourier thermal response in a single layer skin tissue.

For one calming period in deformable structures, Youssef updated Chen and Gurtin's principle of thermal actions. Two specific temperatures are the thermodynamic temperature and the conductive temperature in this device<sup>30,31</sup>. The disparity in the meaning of these two temperature forms is commensurate with the importance of the material's thermal supply. Youssef with El-Bary and Alghamdi applied the two-temperature heat conduction in many applications<sup>32-37</sup>.

In the present paper, a mathematical model of bioheat skin tissue will be constructed in the context of a two-temperature dual-phase-lag heat conduction model. The surface of the skin tissue is subjected to a constant heat flux. The separation of variables as a finite domain will be applied to obtain the exact analytical solution. The effects of the dual-phase-lag time parameter, value of the heat flux, and two-temperature parameter will be studied and discussed.

**Bioheat transfer models for biological tissues.** The bioheat transmitting model was developed to measure the time-dependent temperature change as a heat reaction due to the usage of either heat source or thermal heating. The first model of biological tissues was found out by Pennes based on Fourier's law of heat conduction as follows<sup>28,36,37</sup>:

$$K\nabla^2 T = \rho C \frac{\partial T}{\partial t} - \rho_b w_b C_b (T_b - T) - (Q_{met} + Q_{ext}), \quad (1)$$

where  $\rho$ ,  $C$  and  $K$  are the density, specific heat, and thermal conductivity of the tissue, respectively.  $C_b$ ,  $w_b$ ,  $\rho_b$  and  $T_b$  denote the specific heat of the blood, blood perfusion rate, blood density, and blood temperature, respectively.  $T$  is the absolute temperature function.  $Q_{met}$  denotes the metabolic heat generated by the chemical reaction inside the tissue, and it is constant, and the external heat source is given by  $Q_{ext} = Q_{ext}(t)$ .  $\nabla^2$  is the well-known Laplace operator.

**The modified Fourier's law of heat conduction.** Ventott and Cattaneo modified the classical Fourier thermal drive law by postulating the concept of finite thermal wave propagation speed and taking the following hyperbolic form of the thermal wave<sup>28,36,37</sup>:

$$K\nabla^2 T = \rho C \left(1 + \tau_q \frac{\partial}{\partial t}\right) \frac{\partial T}{\partial t} + w_b C_b \rho_b \left(1 + \tau_q \frac{\partial}{\partial t}\right) (T - T_b) - \left(1 + \tau_q \frac{\partial}{\partial t}\right) (Q_{met} + Q_{ext}), \quad (2)$$

where  $\tau_q = \frac{\alpha}{c_0^2} > 0$  is a material property and is called the relaxation time parameter, and  $\alpha$  is the thermal diffusivity while  $c_0$  is the speed of the thermal wave inside the medium.

**Dual-phase-lag model (DPL) of bioheat transfer.** The dual-phase-lag (DPL) model based on the dual reaction between the gradient of the temperature  $\nabla T$  and the heat flux  $q$  which modified the well-known classical Fourier's law of heat conduction, thus, we have the following heat conduction equation<sup>28,36,37</sup>:

$$K \left(1 + \tau_T \frac{\partial}{\partial t}\right) \nabla^2 T = \rho C \left(1 + \tau_q \frac{\partial}{\partial t}\right) \frac{\partial T}{\partial t} + w_b C_b \rho_b \left(1 + \tau_q \frac{\partial}{\partial t}\right) (T - T_b) - \left(1 + \tau_q \frac{\partial}{\partial t}\right) (Q_{met} + Q_{ext}) \quad (3)$$

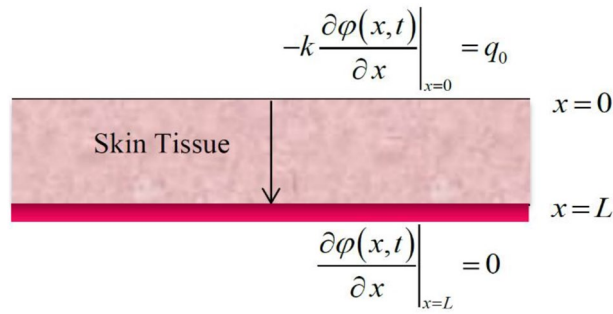


**Figure 1.** The skin tissue affected by constant heat flux on the surface.

where  $\tau_T \geq 0$  is the second parameter of the relaxation time, which is the phase-lag of the temperature gradient passing through the medium.

**Two-temperature dual-phase-lag (TTDPL) bioheat transfer model on skin tissues.** According to Youssef’s model of heat conduction formulation, we have two equations of heat conduction on the biological tissues as following<sup>36,37</sup> :

$$K \left( 1 + \tau_T \frac{\partial}{\partial t} \right) \nabla^2 T_C = \rho C \left( 1 + \tau_q \frac{\partial}{\partial t} \right) \frac{\partial T_D}{\partial t} + w_b C_b \rho_b \left( 1 + \tau_q \frac{\partial}{\partial t} \right) T_D - \left( 1 + \tau_q \frac{\partial}{\partial t} \right) (Q_{met} + Q_{ext}) \quad (4)$$

and

$$T_D = T_C - \beta \nabla^2 T_C \quad (5)$$

where  $\beta$  is a non-negative constant, which is called the two-temperature parameter<sup>36,37</sup>.  $T_D$  and  $T_C$  are the dynamical temperature and the conductive temperature, respectively. The value  $\beta = 0$  represents the one-temperature model, then, we obtain  $T_C = T_D$ .

We consider the function of dynamical temperature increment takes the form

$$\theta = T_D - T_b \quad (6)$$

and the function of conductive temperature increment takes the form

$$\varphi = T_C - T_b \quad (7)$$

Hence, we have

$$K \left( 1 + \tau_T \frac{\partial}{\partial t} \right) \nabla^2 \varphi = \rho C \left( 1 + \tau_q \frac{\partial}{\partial t} \right) \frac{\partial \theta}{\partial t} + w_b C_b \rho_b \left( 1 + \tau_q \frac{\partial}{\partial t} \right) \theta - \left( 1 + \tau_q \frac{\partial}{\partial t} \right) (Q_{met} + Q_{ext}) \quad (8)$$

and

$$\theta = \varphi - \beta \nabla^2 \varphi \quad (9)$$

### Method

We consider the region  $0 \leq x \leq L$  is filled with skin tissue as in Fig. 1 and obeys the two-temperature dual-phase-lag (TTDPL) as in Eqs. (8) and (9).

The medium is considered to be quiescent initially and without any external heat source ( $Q_{ext} = 0$ ) while  $Q_{met}$  is constant. The skin is subjected to a constant heat flux  $q_0$  on its bounding surface  $x = 0$ , while the bounding surface  $x = L$  has no heat flux (see Fig. 1).

Hence, the heat conduction equations take the forms:

$$\left[ \beta \rho C \tau_q \frac{\partial^2}{\partial t^2} + (K \tau_T + \beta \rho C + \beta \tau_q w_b C_b \rho_b) \frac{\partial}{\partial t} + (\beta w_b C_b \rho_b + K) \right] \frac{\partial^2 \varphi}{\partial x^2} = \left( \tau_q \rho C \frac{\partial^2}{\partial t^2} + (\rho C + \tau_q w_b C_b \rho_b) \frac{\partial}{\partial t} + w_b C_b \rho_b \right) \varphi - Q_{met} \quad (10)$$

and

$$\theta = \varphi - \beta \frac{\partial^2 \varphi}{\partial x^2} \quad (11)$$

The initial conditions are:

$$\varphi(x, t)|_{t=0} = \theta(x, t)|_{t=0} = \frac{\partial \varphi(x, t)}{\partial t} \Big|_{t=0} = \frac{\partial \theta(x, t)}{\partial t} \Big|_{t=0} = 0 \tag{12}$$

The boundary conditions are:

$$-K \frac{\partial \varphi(x, t)}{\partial x} \Big|_{x=0} = q_0 \quad \frac{\partial \varphi(x, t)}{\partial x} \Big|_{x=L} = 0 \tag{13}$$

The boundary value problem (10)–(13) consists of non-homogeneous partial differential equations with non-homogeneous boundary conditions on the surface of the skin tissue. Thus, the equations must be formulated in terms of a steady part and a transient part as follows<sup>38,39</sup>:

$$\varphi(x, t) = \phi_1(x, t) + \phi_2(x) \tag{14}$$

Hence, we obtain the transient part in the form

$$\left[ \beta \rho C \tau_q \frac{\partial^2}{\partial t^2} + (K \tau_T + \beta \rho C + \beta \tau_q w_b C_b \rho_b) \frac{\partial}{\partial t} + (\beta w_b C_b \rho_b + K) \right] \frac{\partial^2 \phi_1(x, t)}{\partial x^2} - \left( \tau_q \rho C \frac{\partial^2}{\partial t^2} + (\rho C + \tau_q w_b C_b \rho_b) \frac{\partial}{\partial t} + w_b C_b \rho_b \right) \phi_1(x, t) = 0 \tag{15}$$

and the steady-state part in the form

$$\left( \frac{d^2}{dx^2} - \lambda^2 \right) \phi_2(x) = -\gamma \psi \tag{16}$$

where  $\lambda^2 = \frac{w_b C_b \rho_b}{(\beta w_b C_b \rho_b + K)} > 0$ ,  $\gamma = \frac{1}{(\beta w_b C_b \rho_b + K)} > 0$ , and  $\psi = Q_{met}$ .

The boundary conditions for the steady-state equation are

$$-K \frac{d\phi_2(x)}{dx} \Big|_{x=0} = q_0, \quad -K \frac{d\phi_2(x)}{dx} \Big|_{x=L} = 0 \tag{17}$$

Then, regarding the boundary conditions on (13), the solution of the Eq. (10) is in the form (See “Appendix”):

$$\phi_2(x) = \frac{q_0 \cosh \lambda(L-x)}{\lambda K \sinh \lambda L} + \frac{\gamma}{\lambda^2} \psi \tag{18}$$

The initial and boundary conditions of the transient Eq. (12) are:

$$\phi_1(x, t)|_{t=0} = -\phi_2(x), \quad \frac{\partial \phi_1(x, t)}{\partial t} \Big|_{t=0} = 0 \tag{19}$$

and

$$\frac{\partial \phi_1(x, t)}{\partial x} \Big|_{x=0} = 0, \quad \frac{\partial \phi_1(x, t)}{\partial x} \Big|_{x=L} = 0 \tag{20}$$

To solve the Eq. (15) we expand the function  $\phi_1(x, t)$  in the following Fourier series expansion<sup>38,39</sup>

$$\phi_1(x, t) = \sum_{n=0}^{\infty} \vartheta_n(t) \cos \left( \frac{n\pi}{L} x \right) \tag{21}$$

which satisfies the boundary conditions (20).

Substitute from Eqs. (21) into (15), we get

$$\left[ \frac{\partial^2}{\partial t^2} + A_{1n} \frac{\partial}{\partial t} + A_{2n} \right] \vartheta_n(t) = 0, \quad n = 0, 1, 2, 3 \dots \tag{22}$$

where  $A_{1n} = \frac{\omega_n^2 (\eta \tau_T + \beta + \beta \tau_q \varepsilon) + (1 + \tau_q \varepsilon)}{\tau_q (\beta \omega_n^2 + 1)}$ ,  $A_{2n} = \frac{\omega_n^2 (\beta \varepsilon + \eta) + \varepsilon}{\tau_q (\beta \omega_n^2 + 1)}$ ,  $\varepsilon = \frac{w_b C_b \rho_b}{\rho C}$ ,  $\eta = \frac{K}{\rho C}$  and  $\omega_n = \frac{n\pi}{L}$ .

The general solutions to (22) take the following forms<sup>38,39</sup>:

$$\vartheta_n(t) = a_n f_1(k_{1n}, t) + b_n f_2(k_{2n}, t), \quad n = 0, 1, 2, \dots \tag{23}$$

which give

$$\vartheta_1(x, t) = \sum_{n=0}^{\infty} [a_n f_1(k_{1n}, t) + b_n f_2(k_{2n}, t)] \cos(\omega_n x) \tag{24}$$

where  $k_{1n}, k_{2n}$  is the solution of the following characteristic equation

$$k^2 + A_{1n}k + A_{2n} = 0 \quad (25)$$

The roots of the characteristic Eq. (25) are in the forms:

$$k_{1n} = \frac{-A_{1n} + \sqrt{\Delta_n}}{2}, \quad k_{2n} = \frac{-A_{1n} - \sqrt{\Delta_n}}{2} \quad (26)$$

where  $\Delta_n = A_{1n}^2 - 4A_{2n}$ .

To apply the initial conditions (19), we have to expand  $\phi_2(x)$  in Fourier series expansion to be in the form:

$$\phi_2(x) = \frac{q_0}{2LK\lambda^2} + \frac{\gamma\psi}{2\lambda^2} + \frac{q_0}{KL} \sum_{n=1}^{\infty} \frac{1}{(\lambda^2 + \omega_n^2)} \cos(\omega_n x) \quad (27)$$

Hence, the initial conditions (19) give the following system of algebraic equations:

$$[a_0 f_1(k_{10}, 0) + b_0 f_2(k_{20}, 0)] \cos(\omega_0 x) + \sum_{n=1}^{\infty} [a_n f_1(k_{1n}, 0) + b_n f_2(k_{2n}, 0)] \cos(\omega_n x) = -\phi_2(x) \quad (28)$$

and

$$\left[ a_0 \frac{\partial f_1(k_{10}, 0)}{\partial t} + b_0 \frac{\partial f_2(k_{20}, 0)}{\partial t} \right] \cos(\omega_0 x) + \sum_{n=1}^{\infty} \left[ a_n \frac{\partial f_1(k_{1n}, 0)}{\partial t} + b_n \frac{\partial f_2(k_{2n}, 0)}{\partial t} \right] \cos(\omega_n x) = 0 \quad (29)$$

For the case of  $\Delta_n > 0$

$$f_1(k_{1n}, t) = e^{k_{1n}t} \quad \text{and} \quad f_2(k_{2n}, t) = e^{k_{2n}t} \quad (30)$$

Thus, when  $t = 0$  we have

$$f_1(k_{1n}, 0) = f_2(k_{2n}, 0) = 1, \quad \frac{\partial f_1(k_{1n}, 0)}{\partial t} = k_{1n}, \quad \frac{\partial f_2(k_{2n}, 0)}{\partial t} = k_{2n}, \quad n = 0, 1, 2, 3, \dots$$

Then, Eqs. (28) and (29) introduce the following system

$$[a_0 + b_0] \cos(\omega_0 x) + \sum_{n=1}^{\infty} [a_n + b_n] \cos(\omega_n x) = -\frac{q_0}{2LK\lambda^2} - \frac{\gamma\psi}{2\lambda^2} - \frac{q_0}{KL} \sum_{n=1}^{\infty} \frac{1}{(\lambda^2 + \omega_n^2)} \cos(\omega_n x) \quad (31)$$

and

$$[k_{10}a_0 + k_{20}b_0] \cos(\omega_0 x) + \sum_{n=1}^{\infty} [k_{1n}a_n + k_{2n}b_n] \cos(\omega_n x) = 0 \quad (32)$$

when  $n = 0$  we have

$$\omega_0 = 0, \quad \cos(\omega_0 x) = 1, \quad A_{10} = \frac{\varepsilon\tau_q + 1}{\tau_q}, \quad A_{20} = \frac{\varepsilon}{\tau_q}, \quad \Delta_0 = \left( \frac{\varepsilon\tau_q - 1}{\tau_q} \right)^2, \quad k_{10} = \frac{-1}{\tau_q}, \quad k_{20} = -\varepsilon.$$

Hence, the system in Eqs. (31) and (32) will be reduced to the following system

$$a_0 + b_0 + \sum_{n=1}^{\infty} [a_n + b_n] \cos(\omega_n x) = -\frac{q_0}{2LK\lambda^2} - \frac{\gamma\psi}{2\lambda^2} - \frac{q_0}{LK} \sum_{n=1}^{\infty} \frac{1}{(\lambda^2 + \omega_n^2)} \cos(\omega_n x) \quad (33)$$

and

$$-\frac{a_0}{\tau_q} - \varepsilon b_0 + \sum_{n=1}^{\infty} [k_{1n}a_n + k_{2n}b_n] \cos(\omega_n x) = 0 \quad (34)$$

The equations in (33) and (34) lead to the following two systems of algebraic equations

$$a_0 + b_0 = -\left( \frac{q_0}{2LK\lambda^2} + \frac{\gamma\psi}{2\lambda^2} \right), \quad a_0 + \tau_q \varepsilon b_0 = 0 \quad (35)$$

and

$$a_n + b_n = \frac{-q_0}{LK(\lambda^2 + \omega_n^2)}, \quad k_{1n}a_n + k_{2n}b_n = 0, \quad n = 1, 2, 3, \dots \quad (36)$$

By solving the above two systems, we get

$$a_0 = \left( \frac{\varepsilon\tau_q}{1 - \varepsilon\tau_q} \right) \left( \frac{q_0}{2LK\lambda^2} + \frac{\gamma\psi}{2\lambda^2} \right), \quad b_0 = \left( \frac{-1}{1 - \varepsilon\tau_q} \right) \left( \frac{q_0}{2LK\lambda^2} + \frac{\gamma\psi}{2\lambda^2} \right) \quad (37)$$

and

$$a_n = \left( \frac{k_{2n}}{k_{1n} - k_{2n}} \right) \frac{q_0}{LK(\lambda^2 + \omega_n^2)}, \quad b_n = \left( \frac{-k_{1n}}{k_{1n} - k_{2n}} \right) \frac{q_0}{LK(\lambda^2 + \omega_n^2)}, \quad n = 1, 2, 3 \dots \quad (38)$$

Now, the final solution of the heat conduction temperature increment, in this case, is in the form

$$\varphi(x, t) = \frac{q_0}{2LK\lambda^2} + \frac{\gamma\psi}{2\lambda^2} + \frac{q_0}{KL} \sum_{n=1}^{\infty} \frac{1}{(\lambda^2 + \omega_n^2)} \cos(\omega_n x) + \left( \frac{1}{1 - \varepsilon\tau_q} \right) \left( \frac{q_0}{2LK\lambda^2} + \frac{\gamma\psi}{2\lambda^2} \right) \left[ \varepsilon\tau_q e^{\frac{-t}{\tau_q}} - e^{-\varepsilon t} \right] + \frac{q_0}{KL} \sum_{n=1}^{\infty} \left( \frac{k_{2n}e^{k_{1n}t} - k_{1n}e^{k_{2n}t}}{(k_{1n} - k_{2n})(\lambda^2 + \omega_n^2)} \right) \cos(\omega_n x) \quad (39)$$

By using Eqs. (39) and (11), we get the dynamical temperature increment as follows:

$$\theta(x, t) = \frac{q_0}{2LK\lambda^2} + \frac{\gamma\psi}{2\lambda^2} + \frac{q_0}{KL} \sum_{n=1}^{\infty} \frac{(1 + \beta\omega_n^2)}{(\lambda^2 + \omega_n^2)} \cos(\omega_n x) + \left( \frac{1}{1 - \varepsilon\tau_q} \right) \left( \frac{q_0}{2LK\lambda^2} + \frac{\gamma\psi}{2\lambda^2} \right) \left[ \varepsilon\tau_q e^{\frac{-t}{\tau_q}} - e^{-\varepsilon t} \right] + \frac{q_0}{KL} \sum_{n=1}^{\infty} (1 - \beta\omega_n^2) \left( \frac{k_{2n}e^{k_{1n}t} + k_{1n}e^{k_{2n}t}}{(k_{1n} - k_{2n})(\lambda^2 + \omega_n^2)} \right) \cos(\omega_n x) \quad (40)$$

For the case of  $\Delta < 0$ , we have

$$f_1(k_{1n}, t) = e^{(k_{1n}t)} \cos\left(\frac{\sqrt{-\Delta_n}}{2} t\right), \quad f_2(k_{2n}, t) = e^{(k_{2n}t)} \sin\left(\frac{\sqrt{-\Delta_n}}{2} t\right), \quad (41)$$

$$\frac{\partial f_1(k_{1n}, t)}{\partial t} = e^{(k_{1n}t)} \left[ k_{1n} \cos\left(\frac{\sqrt{-\Delta_n}}{2} t\right) - \frac{\sqrt{-\Delta_n}}{2} \sin\left(\frac{\sqrt{-\Delta_n}}{2} t\right) \right] \quad (42)$$

$$\frac{\partial f_2(k_{2n}, t)}{\partial t} = e^{(k_{2n}t)} \left[ k_{2n} \sin\left(\frac{\sqrt{-\Delta_n}}{2} t\right) + \frac{\sqrt{-\Delta_n}}{2} \cos\left(\frac{\sqrt{-\Delta_n}}{2} t\right) \right] \quad (43)$$

$$f_1(k_{1n}, 0) = 1, \quad f_2(k_{2n}, 0) = 0, \quad n = 0, 1, 2, 3 \dots \quad (44)$$

$$\frac{\partial f_1(k_{1n}, 0)}{\partial t} = k_{1n}, \quad \frac{\partial f_2(k_{2n}, 0)}{\partial t} = \frac{\sqrt{-\Delta_n}}{2}, \quad n = 0, 1, 2, 3 \dots \quad (45)$$

$$A_{10} = \frac{1}{\tau_q}, \quad A_{20} = \frac{\varepsilon}{\tau_q}, \quad \Delta_0 = \left( \frac{\varepsilon\tau_q - 1}{\tau_q} \right)^2, \quad k_{10} = \frac{-1}{\tau_q}, \quad k_{20} = -\varepsilon$$

Applying the initial conditions (19), we obtain

$$a_0 + \sum_{n=1}^{\infty} a_n \cos(\omega_n x) = -\frac{q_0}{2LK\lambda^2} - \frac{\gamma\psi}{2\lambda^2} - \frac{q_0}{KL} \sum_{n=1}^{\infty} \frac{1}{(\lambda^2 + \omega_n^2)} \cos(\omega_n x) \quad (46)$$

and

$$\left( -\frac{1}{\tau_q} \right) a_0 + \left( \frac{\tau_q - 1}{2\tau_q} \right) b_0 + \sum_{n=1}^{\infty} \left[ a_n k_{1n} + b_n \frac{\sqrt{-\Delta_n}}{2} \right] \cos(\omega_n x) = 0 \quad (47)$$

Solving the above system, we obtain

$$a_0 = -\left( \frac{q_0}{2LK\lambda^2} + \frac{\gamma\psi}{2\lambda^2} \right), \quad b_0 = -\left( \frac{1}{\tau_q - 1} \right) \left( \frac{q_0}{LK\lambda^2} + \frac{\gamma\psi}{\lambda^2} \right) \quad (48)$$

$$a_n = -\frac{q_0}{KL(\lambda^2 + \omega_n^2)}, \quad b_n = \frac{2k_{1n}q_0}{KL(\lambda^2 + \omega_n^2)\sqrt{-\Delta_n}} \quad (49)$$

Parameter	Unit	Skin	Parameter	Unit	Skin
$K$	$W/m^{\circ}C$	0.215	$W_b$	$ml/Cm$	0.00052
$\rho$	$kg/m^3$	1000	$T_b$	$^{\circ}C$	37
$\rho_b$	$kg/m^3$	1060	$\tau_T$	$s$	10.0
$C$	$J/kg^{\circ}C$	4187	$\tau_q$	$s$	20.0
$C_b$	$J/kg^{\circ}C$	3800	$L$	$m$	0.006

**Table 1.** The material properties of the skin tissue.

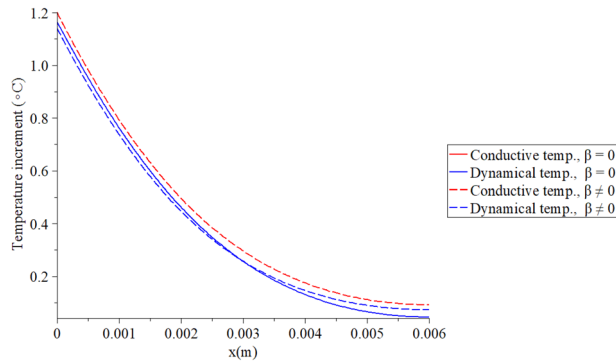


**Figure 2.** The temperature increment when  $t = 100$  (s),  $\tau_T = 10$  (s),  $\tau_q = 20$  (s) and  $q_0 = 100$  ( $W/m^2$ ).

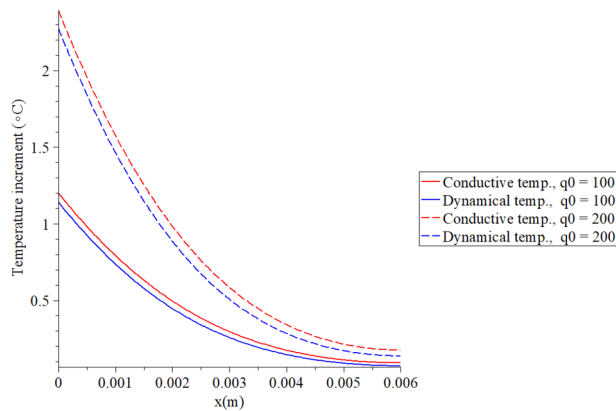


**Figure 3.** The temperature increment when  $t = 100$  (s),  $\tau_T = 10$  (s),  $\tau_q = 20$  (s) and various values of the surface heat flux  $q_0$  ( $W/m^2$ ) based on the two-temperature model.

Hence, the final solution of the heat conduction temperature increment in this case is:

$$\begin{aligned}
 \varphi(x, t) = & \frac{q_0}{2LK\lambda^2} + \frac{\psi}{2} + \frac{q_0}{KL} \sum_{n=1}^{\infty} \frac{1}{(\lambda^2 + \omega_n^2)} \cos(\omega_n x) - \left( \frac{q_0}{2LK\lambda^2} + \frac{\gamma\psi}{2\lambda^2} \right) e^{\frac{-t}{\tau_q}} \cos\left(\frac{\sqrt{-\Delta_0}}{2} t\right) \\
 & - \left( \frac{1}{\tau_q - 1} \right) \left( \frac{q_0}{LK\lambda^2} + \frac{\gamma\psi}{\lambda^2} \right) e^{-t} \sin\left(\frac{\sqrt{-\Delta_0}}{2} t\right) + \frac{q_0}{KL} \sum_{n=1}^{\infty} \left[ e^{(k_{1n} t)} \cos\left(\frac{\sqrt{-\Delta_n}}{2} t\right) \right. \\
 & \left. + \frac{2k_{1n}}{\sqrt{-\Delta_n}} e^{(k_{2n} t)} \sin\left(\frac{\sqrt{-\Delta_n}}{2} t\right) \right] \frac{\cos(\omega_n x)}{(\lambda^2 + \omega_n^2)} \quad (50)
 \end{aligned}$$

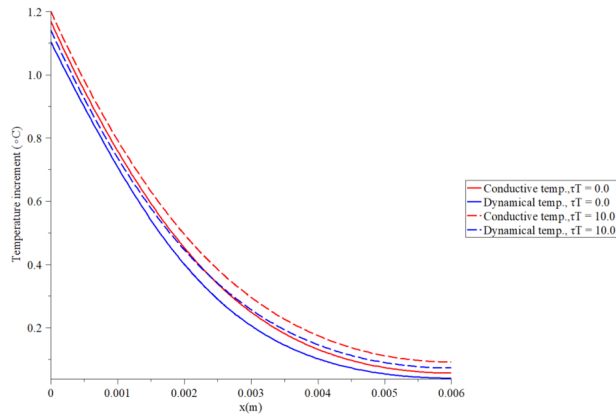


**Figure 4.** The temperature increment when  $t = 100$  (s),  $q_0 = 100$  (W/m<sup>2</sup>),  $\tau_q = 20$  (s) and various values  $\tau_T$ (s) based on the two-temperature model.

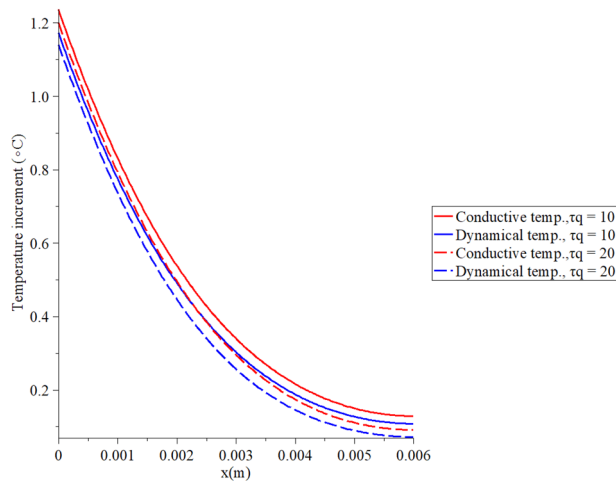


**Figure 5.** The temperature increment when  $t = 100$  (s),  $q_0 = 100$  (W/m<sup>2</sup>),  $\tau_T = 10$  (s) and various values  $\tau_q$ (s) based on the two-temperature model.

By using Eqs. (50) and (11), we get the dynamical temperature increment in this case as follows:

$$\begin{aligned} \theta(x, t) = & \frac{q_0}{2LK\lambda^2} + \frac{\psi}{2} + \frac{q_0}{KL} \sum_{n=1}^{\infty} \frac{(1 + \omega_n^2\beta)}{(\lambda^2 + \omega_n^2)} \cos(\omega_n x) - \left( \frac{q_0}{2LK\lambda^2} + \frac{\gamma\psi}{2\lambda^2} \right) e^{-\frac{t}{\tau_q}} \cos\left(\frac{\sqrt{-\Delta_0}}{2} t\right) \\ & - \left( \frac{1}{\tau_q - 1} \right) \left( \frac{q_0}{LK\lambda^2} + \frac{\gamma\psi}{\lambda^2} \right) e^{-t} \sin\left(\frac{\sqrt{-\Delta_0}}{2} t\right) + \frac{q_0}{KL} \sum_{n=1}^{\infty} \left[ e^{(k_{1n} t)} \cos\left(\frac{\sqrt{-\Delta_n}}{2} t\right) \right. \\ & \left. + \frac{2k_{1n}}{\sqrt{-\Delta_n}} e^{(k_{2n} t)} \sin\left(\frac{\sqrt{-\Delta_n}}{2} t\right) \right] \frac{(1 + \omega_n^2\beta) \cos(\omega_n x)}{(\lambda^2 + \omega_n^2)} \end{aligned} \quad (51)$$

### Results

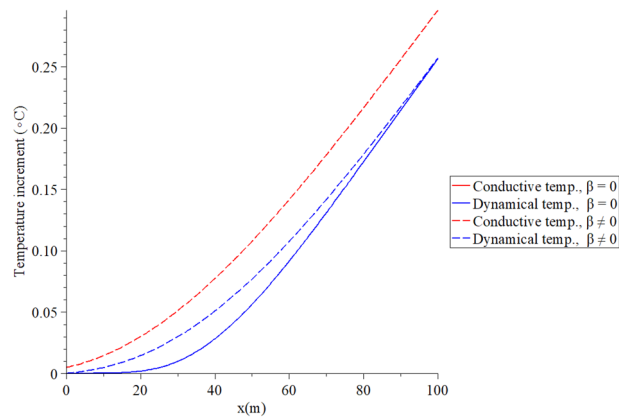
In this study, the temperature distribution through skin tissue is investigated for two models (One temperature, two temperature) of bioheat transfer for constant heat flux condition on the skin surface. The values of the relevant thermal parameters used in the present calculations are in Table 1 as follows:

### Discussions

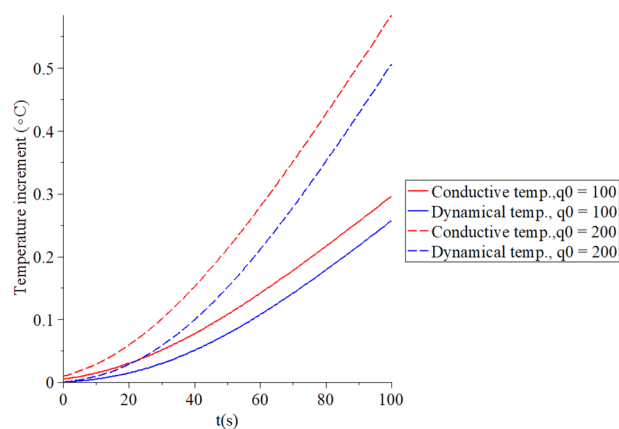
Figures 2, 3, 4, 5 represent the conductive and dynamical temperature increment with respect to a wide range of skin distance  $x$  ( $0 \leq x \leq 0.006$  m) and at constant instance time  $t = 100$ (s).

Figure 2 shows that the two temperature parameter  $\beta$  has a significant effect on the temperature increment distribution. The red line represents the conductive temperature distribution, while the blue line represents the dynamical temperature distribution. The conductive temperature increment and dynamical temperature





**Figure 6.** The temperature increment when  $x = 0.003$  (m),  $\tau_T = 10$  (s),  $\tau_q = 20$  (s) and  $q_0 = 100$  ( $W/m^2$ ).



**Figure 7.** The temperature increment when  $x = 0.003$  (m),  $\tau_T = 10$  (s),  $\tau_q = 20$  (s) and various values of the surface heat flux  $q_0$  ( $W/m^2$ ) based on the two-temperature model.

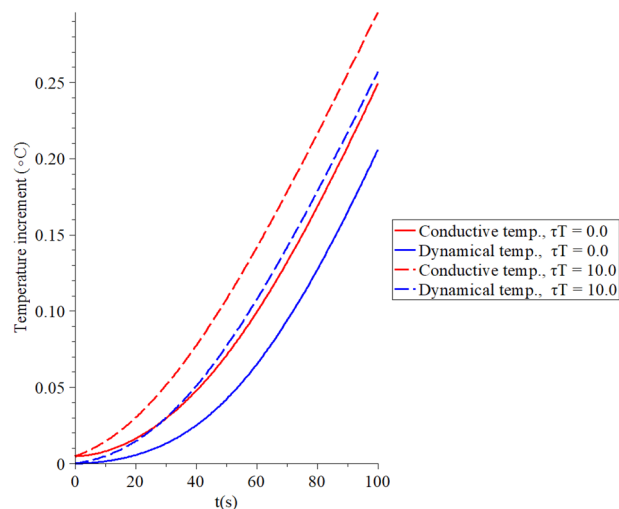


**Figure 8.** The temperature increment when  $x = 0.003$  (m),  $q_0 = 100$  ( $W/m^2$ ),  $\tau_q = 20$  (s) and various values  $\tau_T$  (s) based on the two-temperature model.

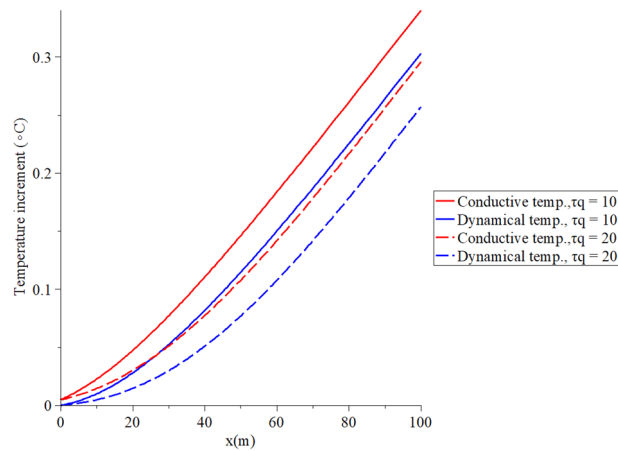


**Figure 9.** The temperature increment when  $x = 0.003$  (m),  $q_0 = 100$  ( $\text{W}/\text{m}^2$ ),  $\tau_T = 10$  (s) and various values  $\tau_q$ (s) based on the two-temperature model.

increment have the same behavior but with different values because of the effect of the two-temperature parameter. In the context of the one-temperature model  $\beta = 0$ , the conductive and dynamical temperature increments are the same, and they appear in the solid blue curve. It is noted that an increase in the value of the two-temperature parameter leads to an increase in the value of conductive temperature increment and a decrease in the value of dynamical temperature increment. We noticed that thermal waves in the context of the one-temperature model have vanished before the thermal waves in the context of the two-temperature model.

Figure 3 shows that the conductive and dynamical temperature increment distributions when  $t = 100$  (s),  $\tau_T = 10$  (s),  $\tau_q = 20$  (s) and various values of the surface heat flux  $q_0$  ( $\text{W}/\text{m}^2$ ) = (100, 200) to stand on its effects. It is noted that the value of the heat flux on the surface of the skin tissue has a significant impact on the conductive and dynamical temperature increment distributions. An increase in the value of the heat flux leads to an increase in the value of the conductive and dynamical temperature increment distributions. A smaller value of the surface heat flux makes the temperature more closed to zero value at the end of the skin length.

Figure 4 shows that the conductive and dynamical temperature increment distributions when  $t = 100$  (s),  $q_0 = 100$  ( $\text{W}/\text{m}^2$ ),  $\tau_q = 20$  (s) and various values of the second relaxation time parameter  $\tau_T$ (s) = (0.0, 10.0) to stand on its effects. It is noted that the value of the second relaxation time parameter has a significant impact on the conductive and dynamical temperature increment distributions. An increase in the value of the second relaxation time parameter leads to an increase in the value of the conductive and dynamical temperature increment distributions. The zero value of the first relaxation time parameter  $\tau_T$  (temperature lag-time) makes the thermal waves more closed to the zero value at the end of the skin length.

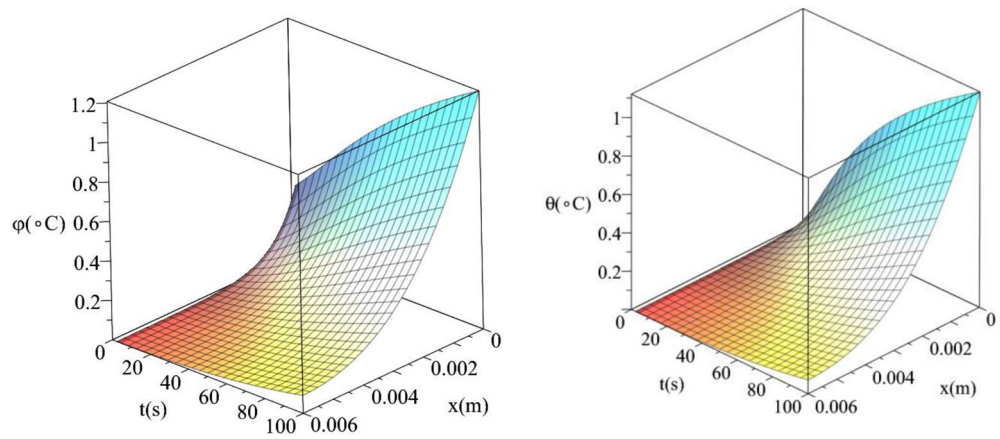
Figure 5 shows that the conductive and dynamical temperature increment distributions when  $t = 100$  (s),  $q_0 = 100$  ( $\text{W}/\text{m}^2$ ),  $\tau_T = 10$  (s) and various values of the first relaxation time parameter  $\tau_q$ (s) = (10, 20) to stand on its effects. It is noted that the value of the first relaxation time  $\tau_q$  parameter has noticeable effects on the conductive and dynamical temperature increment distributions. An increase in the value of the second relaxation time parameter  $\tau_q$  leads to a decrease in the value of the conductive and dynamical temperature increment distributions. Increasing the value of the second relaxation time parameter  $\tau_q$ (temperature gradient lag-time) makes the thermal waves more closed to the zero value at the end of the skin length.

Figures 6, 7, 8, 9 represent the conductive and dynamical temperature increment with respect to a wide range of time  $x$  ( $0 \leq t \leq 100$  s) and at a constant distance  $x = 0.003$ (m).

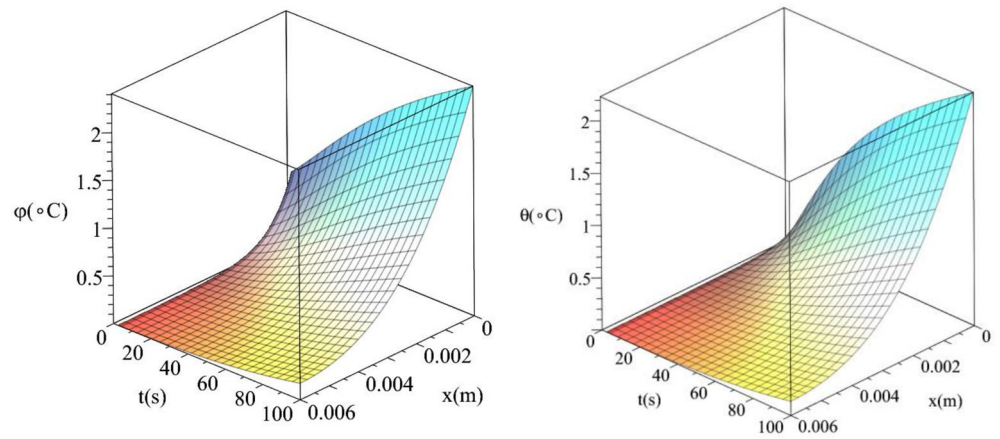
Figure 6 shows that the two temperature parameter  $\beta$  has a significant effect on the temperature increment distribution. The conductive temperature increment and dynamical temperature increment have the same behavior but with different values because of the impact of the two-temperature parameter. In the context of the one-temperature model  $\beta = 0$ , the conductive and dynamical temperature increments are the same, and the solid blue curve represents them. It is noted that an increase in the value of the two-temperature parameter leads to an increase in the value of conductive temperature increment and a decrease in the value of dynamical temperature increment.

Figure 7 shows that the conductive and dynamical temperature increment distributions when  $x = 0.003$  (m),  $\tau_T = 10$  (s),  $\tau_q = 20$  (s) and various values of the surface heat flux  $q_0$  ( $\text{W}/\text{m}^2$ ) = (100, 200) to stand on its effects. It is noted that the value of the heat flux on the surface of the skin tissue has a significant impact on the conductive and dynamical temperature increment distributions. An increase in the value of the heat flux leads to an increase in the value of the conductive and dynamical temperature increment distributions.

Figure 8 shows that the conductive and dynamical temperature increment distributions when  $x = 0.003$  (m),  $q_0 = 100$  ( $\text{W}/\text{m}^2$ ),  $\tau_q = 20$  (s) and various values of the second relaxation time parameter  $\tau_T$ (s) = (0.0, 10.0) to stand on its effects. It is noted that the value of the second relaxation time parameter has a significant impact on the conductive and dynamical temperature increment distributions. An increase in the value of the second relaxation time parameter leads to an increase in the value of the conductive and dynamical temperature increment distributions.



**Figure 10.** The conductive and dynamical temperature increment when  $q_0 = 100(\text{W}/\text{m}^2)$  based on the two-temperature model.



**Figure 11.** The conductive and dynamical temperature increment when  $q_0 = 200(\text{W}/\text{m}^2)$  based on the two-temperature model.

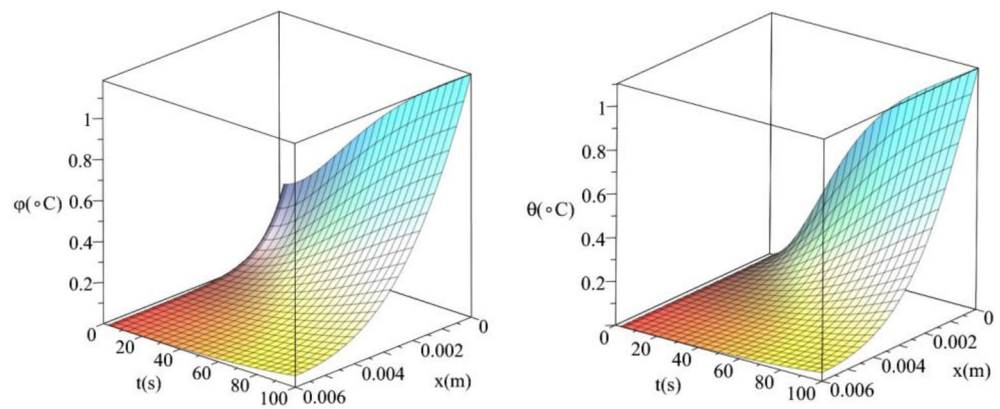


**Figure 12.** The conductive and dynamical temperature increment when  $\tau_T (s) = 0.0$  based on the two-temperature model.

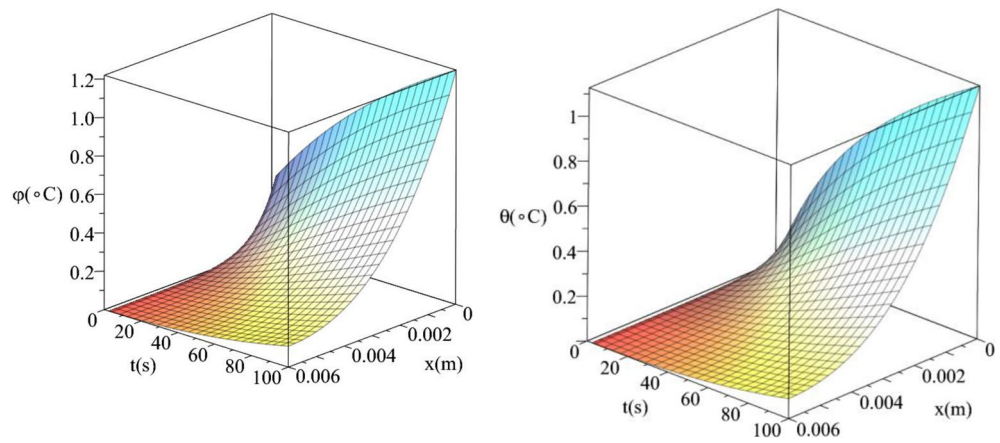


**Figure 13.** The conductive and dynamical temperature increment when  $\tau_T$  (s) = 15 based on the two-temperature model.

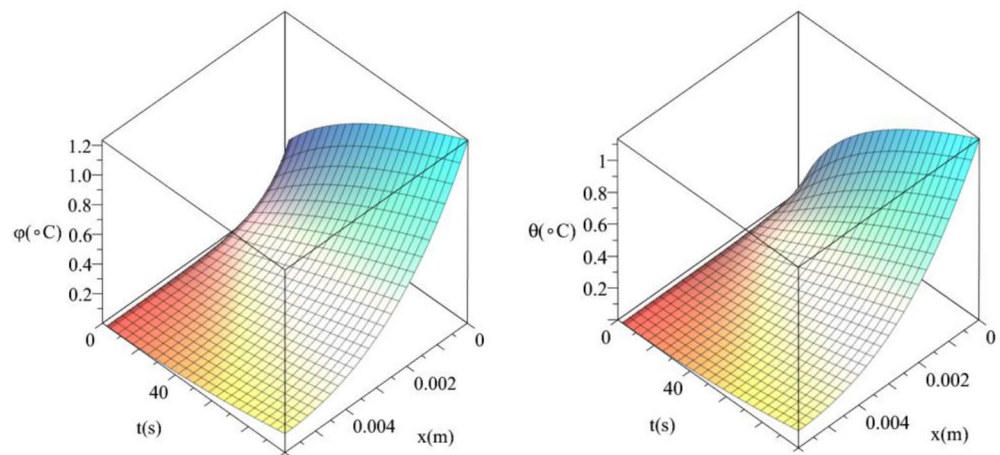


**Figure 14.** The conductive and dynamical temperature increment when  $\tau_q$  (s) = 10.

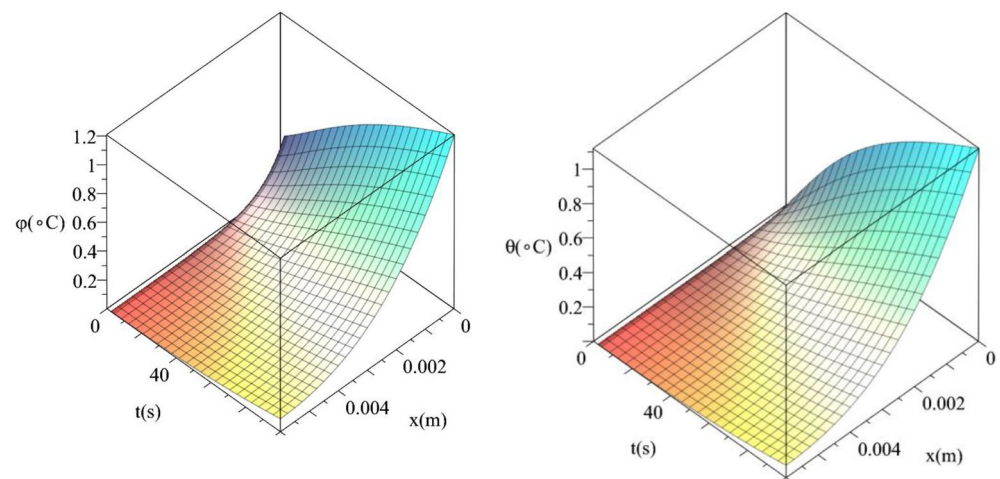


**Figure 15.** The conductive and dynamical temperature increment when  $\tau_q$  (s) = 20.

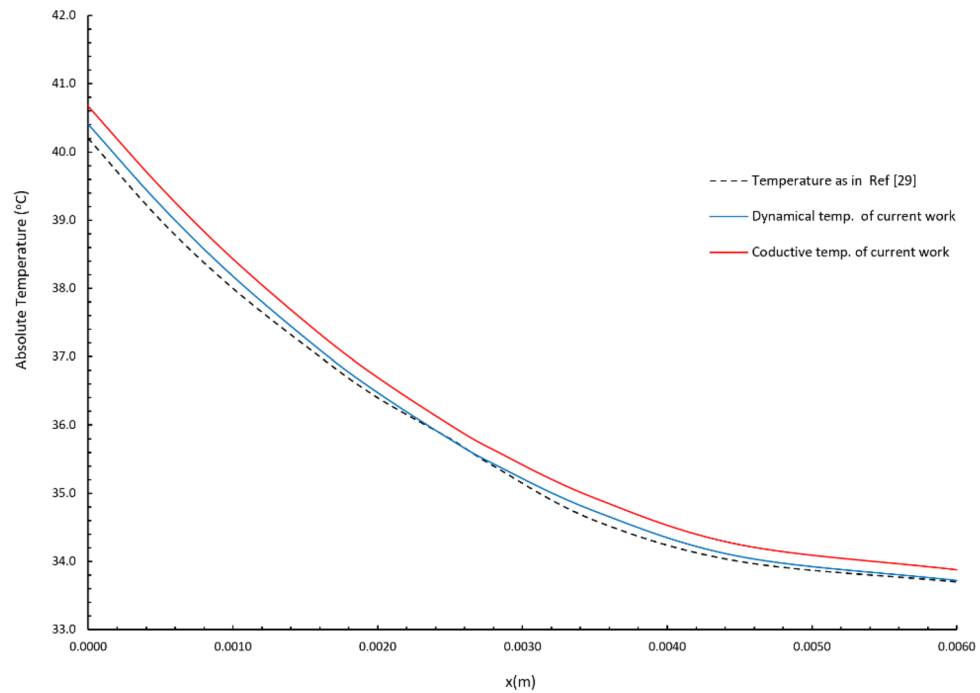


**Figure 16.** The absolute conductive and dynamical temperatures of the current model against Kundu and Dewanjee<sup>29</sup> when  $\rho_b W_b = 0.5 \text{ kg/m}^3 \text{ s}$ ,  $\tau_T = 0$ ,  $\tau_q = 20 \text{ s}$ ,  $K = 0.2 \text{ W/m}^\circ\text{C}$ ,  $t = 160 \text{ s}$ ,  $q_0 = 500 \text{ W/m}^2$ .

Figure 9 shows that the conductive and dynamical temperature increment distributions when  $x(m) = 0.003$ ,  $q_0 (\text{W/m}^2) = 100$ ,  $\tau_T (\text{s}) = 10$  and various values of the second relaxation time parameter  $\tau_q (\text{s}) = (0.0, 10.0)$  to stand on its effects. It is noted that the value of the first relaxation time parameter has a significant impact on the conductive and dynamical temperature increment distributions. An increase in the value of the first relaxation time parameter leads to a decrease in the value of the conductive and dynamical temperature increment distributions.

Figures 10 and 11 show the differences between the conductive temperature increment and dynamical temperature increment with respect to a wide range of time  $t (0 \leq t \leq 100 (\text{s}))$  and distance  $x (0 \leq x \leq 0.006 (\text{m}))$ . Figure 8 represents the conductive temperature increment and dynamical temperature increment when  $q_0 (\text{W/m}^2) = 100$  and Fig. 9 when  $q_0 (\text{W/m}^2) = 200$ . These two figures agree with the results in Figs. 3 and 6 and confirm that the value of the heat flux on the surface of the skin tissue has significant effects on the conductive and dynamical temperature increment distributions.

Figures 12 and 13 show the differences between the conductive temperature increment and dynamical temperature increment with respect to a wide range of time  $t (0 \leq t \leq 100 (\text{s}))$  and distance  $x (0 \leq x \leq 0.006 (\text{m}))$  for various values of the second relaxation time parameter  $\tau_T (\text{s}) = (0.0, 10.0)$ . This two figures agree with the results in the Figs. 4 and 7 and confirm that the value of the second relaxation time parameter has significant effects on the conductive and dynamical temperature increment distributions.

Figures 14 and 15 show the differences between the conductive temperature increment and dynamical temperature increment with respect to a wide range of time  $t (0 \leq t \leq 100 (\text{s}))$  and distance  $x (0 \leq x \leq 0.006 (\text{m}))$  for various values of the first relaxation time parameter  $\tau_q (\text{s}) = (10, 20)$ . These two figures agree with the results in Figs. 5 and 9 and confirm that the value of the first relaxation time parameter has significant effects on the conductive and dynamical temperature increment distributions.

Here, we should refer to the agreement of the results of this research with the results of other researches in order to confirm the validity of the current results and the validity of the proposed mathematical model as well as the method of solution.

The current results agree with the results of Youssef and Alghamdi<sup>28,37</sup>. Moreover, the current results agree with the result in figure 6 of Kundu and Dewanjee<sup>29</sup> for the case of boundary condition of cas (b). To verify our results with the results in Kundu and Dewanjee<sup>29</sup>, we represented Fig. 16 in which we use the same values of the parameters in Kundu and Dewanjee<sup>29</sup> as follows:

$$\rho_b W_b = 0.5 \text{ kg/m}^3 \text{ s}, \tau_T = 0, \tau_q = 20 \text{ s}, K = 0.2 \text{ W/m}^\circ\text{C}, t = 160 \text{ s}, q_0 = 500 \text{ W/m}^2$$

and calculating the absolute values of the dynamical and conductive temperature by adding  $T_b = 37^\circ\text{C}$  to the increments as follows:

$$T_D = (\theta + T_b), \quad T_C = (\varphi + T_b)$$



Figure 16 show that the current result of the absolute dynamical and conductive temperature are close to the values of the absolute temperature in Kundu and Dewanjee<sup>29</sup>. Thus, we have a guarantee that the results of the current research are correct and verified.

### Conclusion

- The dual-phase lag time parameters  $\tau_T$ ,  $\tau_q$  have significant effects on the conductive and the dynamical temperature increment of the skin tissue.
- The initial heat flux applying on the surface of the skin tissue has significant on the conductive and the dynamical temperature increment.
- The two-temperature parameter has a significant effect on the conductive and the dynamical temperature increment.
- The Two-temperature dual-phase-lag (TTDPL) bioheat transfer model is a successful model to simulate the thermal behavior of the skin tissue.
- The results in the current work agree with the results of Kundu and Dewanjee<sup>29</sup>. Therefore, the two-temperature dual-phase-lag (TTDPL) bioheat transfer model be a successful model to study the bioheat transfer of a skin tissue and supplies us with exact solutions.

### Appendix

Substituting from Eqs. (14) into (10), we have

$$\begin{aligned} & \left[ \beta \rho C \tau_q \frac{\partial^2}{\partial t^2} \frac{\partial^2}{\partial x^2} + (K \tau_T + \beta \rho C + \beta \tau_q w_b C_b \rho_b) \frac{\partial}{\partial t} \frac{\partial^2}{\partial x^2} + (\beta w_b C_b \rho_b + K) \frac{\partial^2}{\partial x^2} \right] [\phi_1(x, t) + \phi_2(x)] \\ & = \left( \tau_q \rho C \frac{\partial^2}{\partial t^2} + (\rho C + \tau_q w_b C_b \rho_b) \frac{\partial}{\partial t} + w_b C_b \rho_b \right) [\phi_1(x, t) + \phi_2(x)] - \psi \end{aligned} \tag{52}$$

which gives

$$\begin{aligned} & \left[ \beta \rho C \tau_q \frac{\partial^2}{\partial t^2} \frac{\partial^2 \phi_1}{\partial x^2} + (K \tau_T + \beta \rho C + \beta \tau_q w_b C_b \rho_b) \frac{\partial}{\partial t} \frac{\partial^2 \phi_1}{\partial x^2} + (\beta w_b C_b \rho_b + K) \frac{\partial^2 \phi_1}{\partial x^2} \right] \\ & = (\beta w_b C_b \rho_b + K) \frac{d^2 \phi_2}{dx^2} + \left( \tau_q \rho C \frac{\partial^2 \phi_1}{\partial t^2} + (\rho C + \tau_q w_b C_b \rho_b) \frac{\partial \phi_1}{\partial t} + w_b C_b \rho_b \phi_1 \right) + w_b C_b \rho_b \phi_2 - \psi \end{aligned} \tag{53}$$

The Eq. (53) could be separated into two differential equation, one is a partial differential equation of two variables  $x$  and  $t$ , while the second one is ordinary differential equation of one variable  $x$  only as follows:

$$\begin{aligned} & \left[ \beta \rho C \tau_q \frac{\partial^2}{\partial t^2} \frac{\partial^2 \phi_1}{\partial x^2} + (K \tau_T + \beta \rho C + \beta \tau_q w_b C_b \rho_b) \frac{\partial}{\partial t} \frac{\partial^2 \phi_1}{\partial x^2} + (\beta w_b C_b \rho_b + K) \frac{\partial^2 \phi_1}{\partial x^2} \right] \\ & = \left( \tau_q \rho C \frac{\partial^2 \phi_1}{\partial t^2} + (\rho C + \tau_q w_b C_b \rho_b) \frac{\partial \phi_1}{\partial t} + w_b C_b \rho_b \phi_1 \right) \end{aligned} \tag{54}$$

and

$$(\beta w_b C_b \rho_b + K) \frac{d^2 \phi_2}{dx^2} = w_b C_b \rho_b \phi_2 - \psi \tag{55}$$

The differentia Eq. (55) is the steady-state part and it takes the form

$$\left( \frac{d^2}{dx^2} - \lambda^2 \right) \phi_2(x) = -\gamma \psi \tag{56}$$

where  $\lambda^2 = \frac{w_b C_b \rho_b}{(\beta w_b C_b \rho_b + K)} > 0$ ,  $\gamma = \frac{1}{(\beta w_b C_b \rho_b + K)} > 0$ , and  $\psi = Q_{met}$ .  
The boundary conditions for the steady-state (17) take the form

$$\frac{d\phi_2(x)}{dx} = \begin{cases} -\frac{q_0}{K} & \text{for } x = 0 \\ 0 & \text{for } x = L \end{cases} \tag{57}$$

The general solution of (56) takes the form

$$\phi_2(x) = C_1 \cosh(\lambda x) + C_2 \sinh(\lambda x) + \frac{\gamma}{\lambda^2} \psi \tag{58}$$

Applying the boundary conditions (57) as follows:

$$\frac{d\phi_2}{dx} \Big|_{x=0} = C_1 \lambda \sinh(\lambda x) + C_2 \lambda \cosh(\lambda x) \Big|_{x=0} = -\frac{q_0}{K} \tag{59}$$

and

$$\left. \frac{d\phi_2}{dx} \right|_{x=L} = C_1 \lambda \sinh(\lambda x) + C_2 \lambda \cosh(\lambda x)|_{x=L} = 0 \quad (60)$$

Hence, we have

$$C_2 = -\frac{q_0}{K\lambda} \quad (61)$$

and

$$C_1 = -C_2 \frac{\cosh(\lambda L)}{\sinh(\lambda L)} = \frac{q_0}{K\lambda} \frac{\cosh(\lambda L)}{\sinh(\lambda L)} \quad (62)$$

Finally, we have

$$\phi_2(x) = \frac{q_0}{K\lambda} \frac{\cosh(\lambda L)}{\sinh(\lambda L)} \cosh(\lambda x) - \frac{q_0}{K\lambda} \sinh(\lambda x) + \frac{\gamma}{\lambda^2} \psi \quad (63)$$

The last equation after simplification will take the form

$$\phi_2(x) = \frac{q_0 \cosh \lambda(L-x)}{K\lambda \sinh \lambda L} + \frac{\gamma}{\lambda^2} \psi \quad (64)$$

Received: 16 April 2020; Accepted: 9 September 2020

Published online: 29 September 2020

## References

- Xu, F., Lu, T., Seffen, K. & Ng, E. Mathematical modeling of skin bioheat transfer. *Appl. Mech. Rev.* **62**, 050801 (2009).
- Pennes, H. H. Analysis of tissue and arterial blood temperatures in the resting human forearm. *J. Appl. Physiol.* **1**, 93–122 (1948).
- Cattaneo, C. A form of heat-conduction equations which eliminates the paradox of instantaneous propagation. *Compt. Rendu.* **247**, 431 (1958).
- Vernotte, P. Les paradoxes de la theorie continue de l'equation de la chaleur. *Compt. Rendu* **246**, 3154–3155 (1958).
- Xu, F., Lu, T. & Seffen, K. Biothermomechanical behavior of skin tissue. *Acta. Mech. Sin.* **24**, 1–23 (2008).
- Xu, F., Seffen, K. & Lu, T. Non-Fourier analysis of skin biothermomechanics. *Int. J. Heat Mass Transf.* **51**, 2237–2259 (2008).
- Rossmann, C. & Haemmerich, D. Review of temperature dependence of thermal properties, dielectric properties, and perfusion of biological tissues at hyperthermic and ablation temperatures. *Crit. Rev.™ Biomed. Eng.* **42**, 467–492 (2014).
- Moradi, A., Poor, H. Z. & Moosavi, H. Analysis of the DPL bio-heat transfer equation with constant and time-dependent heat flux conditions on skin surface. *Therm. Sci.* **20**, 1457–1472 (2014).
- Tzou, D. Y. A unified field approach for heat conduction from macro-to micro-scales. *J. Heat Transf.* **117**, 8–16 (1995).
- Jou, D. & Tzou, D. Y. Macro-to microscale heat transfer. The lagging behaviour. Series in chemical and mechanical engineering. *J. Non Equilib. Thermodyn.* **23**, 192–193 (1998).
- Ozisik, M. & Tzou, D. On the wave theory in heat conduction. *J. Heat Transf.* **116**, 526–535 (1994).
- Askarizadeh, H. & Ahmadikia, H. Analytical analysis of the dual-phase-lag model of bioheat transfer equation during transient heating of skin tissue. *Heat Mass Transf.* **50**, 1673–1684 (2014).
- Dutta, J. & Kundu, B. Exact analysis based on BDLTNE approach for thermal behaviour in living tissues during regional hyperthermia therapy. *Acta Mech.* **230**, 2853–2871 (2019).
- Liu, K.-C., Wang, Y.-N. & Chen, Y.-S. Investigation on the bio-heat transfer with the dual-phase-lag effect. *Int. J. Therm. Sci.* **58**, 29–35 (2012).
- Liu, K.-C. & Chen, H.-T. Analysis for the dual-phase-lag bio-heat transfer during magnetic hyperthermia treatment. *Int. J. Heat Mass Transf.* **52**, 1185–1192 (2009).
- Liu, K.-C., Chen, H.-T. & Cheng, P.-J. Inverse investigation of non-Fourier heat conduction in tissue. *J. Therm. Biol* **62**, 123–128 (2016).
- Liu, K.-C. & Chen, H.-T. Investigation for the dual phase lag behavior of bio-heat transfer. *Int. J. Therm. Sci.* **49**, 1138–1146 (2010).
- Zhang, Y. Generalized dual-phase lag bioheat equations based on nonequilibrium heat transfer in living biological tissues. *Int. J. Heat Mass Transf.* **52**, 4829–4834 (2009).
- Dutta, J. & Kundu, B. Thermal wave propagation in blood perfused tissues under hyperthermia treatment for unique oscillatory heat flux at skin surface and appropriate initial condition. *Heat Mass Transf.* **54**, 3199–3217 (2018).
- Agrawal, M. & Pardasani, K. Finite element model to study temperature distribution in skin and deep tissues of human limbs. *J. Therm. Biol.* **62**, 98–105 (2016).
- Kumar, D. & Rai, K. Numerical simulation of time fractional dual-phase-lag model of heat transfer within skin tissue during thermal therapy. *J. Therm. Biol.* **67**, 49–58 (2017).
- Shao, Y., Arjun, B., Leo, H. & Chua, K. Nano-assisted radiofrequency ablation of clinically extracted irregularly-shaped liver tumors. *J. Therm. Biol* **66**, 101–113 (2017).
- Liu, J. & Xu, L. X. Estimation of blood perfusion using phase shift in temperature response to sinusoidal heating at the skin surface. *IEEE Trans. Biomed. Eng.* **46**, 1037–1043 (1999).
- Shih, T.-C., Yuan, P., Lin, W.-L. & Kou, H.-S. Analytical analysis of the Pennes bioheat transfer equation with sinusoidal heat flux condition on skin surface. *Med. Eng. Phys.* **29**, 946–953 (2007).
- Ahmadikia, H., Fazlali, R. & Moradi, A. Analytical solution of the parabolic and hyperbolic heat transfer equations with constant and transient heat flux conditions on skin tissue. *Int. Commun. Heat Mass Transf.* **39**, 121–130 (2012).
- Horng, T. L., Lin, W. L., Liauh, C. T. & Shih, T. C. Effects of pulsatile blood flow in large vessels on thermal dose distribution during thermal therapy. *Med. Phys.* **34**, 1312–1320 (2007).
- Shih, T.-C. *et al.* Numerical analysis of coupled effects of pulsatile blood flow and thermal relaxation time during thermal therapy. *Int. J. Heat Mass Transf.* **55**, 3763–3773 (2012).
- Youssef, H. M. & Alghamdi, N. A. Modeling of one-dimensional thermoelastic dual-phase-lag skin tissue subjected to different types of thermal loading. *Sci. Rep.* **10**, 1–12 (2020).
- Kundu, B. & Dewanjee, D. A new method for non-Fourier thermal response in a single layer skin tissue. *Case Stud. Therm. Eng.* **5**, 79–88 (2015).

30. Chen, P. J., Gurtin, M. E. & Williams, W. O. On the thermodynamics of non-simple elastic materials with two temperatures. *Zeitschrift für angewandte Mathematik und Physik ZAMP* **20**, 107–112 (1969).
31. Youssef, H. Theory of two-temperature-generalized thermoelasticity. *IMA J. Appl. Math.* **71**, 383–390 (2006).
32. Youssef, H. M. & Alghamdi, N. Thermoelastic damping in nanomechanical resonators based on two-temperature generalized thermoelasticity theory. *J. Therm. Stresses* **38**, 1345–1359 (2015).
33. Youssef, H. M. & El-Bary, A. Two-temperature generalized thermo-elastic medium thermally excited by time exponentially decaying laser pulse. *Int. J. Struct. Stab. Dyn.* **16**, 1450102 (2016).
34. Youssef, H. State-space approach to two-temperature generalized thermoelasticity without energy dissipation of medium subjected to moving heat source. *Appl. Math. Mech.* **34**, 63–74 (2013).
35. Youssef, H. M. State-space approach to fractional order two-temperature generalized thermoelastic medium subjected to moving heat source. *Mech. Adv. Mater. Struct.* **20**, 47–60 (2013).
36. Youssef, H. M. & Alghamdi, N. Characterization of thermal damage due to two-temperature high-order thermal lagging in a three-dimensional biological tissue subjected to a rectangular laser pulse. *Polymers* **12**, 922 (2020).
37. Youssef, H. M. & Alghamdi, N. A. Three-dimensional biological tissue under high-order effect of two-temperature thermal lagging to thermal responses due to a laser irradiation. *Vibroeng. Procedia* **22**, 112–117 (2019).
38. Kundu, B. Exact analysis for propagation of heat in a biological tissue subject to different surface conditions for therapeutic applications. *Appl. Math. Comput.* **285**, 204–216 (2016).
39. Lin, S.-M. & Li, C.-Y. Analytical solutions of non-Fourier bio-heat conductions for skin subjected to pulsed laser heating. *Int. J. Therm. Sci.* **110**, 146–158 (2016).

## Acknowledgements

The authors are grateful for the support of this work as a part of the project provided by the “Long-Term Comprehensive-National Plan for Science, Technology, and Innovation” through STU of Umm Al-Qura University.

## Author contributions

H. Y. investigated the governing equations, obtained the numerical solutions, represented the results in figures, wrote the draft of the paper, and reviewed all the writing. N. A. proposed the point of the work, wrote the abstract, sheared in the numerical solution, wrote the discussions, and reviewed all the paper.

## Funding

This work was funded by National Science, Technology and Innovation Plan (MAARIFAH), King Abdulaziz City for Science and Technology (KACST), Kingdom of Saudi Arabia, grant number (14-MAT162-10).

## Competing interests

The authors declare no competing interests.

## Additional information

**Correspondence** and requests for materials should be addressed to H.M.Y.

**Reprints and permissions information** is available at [www.nature.com/reprints](http://www.nature.com/reprints).

**Publisher’s note** Springer Nature remains neutral with regard to jurisdictional claims in published maps and institutional affiliations.



**Open Access** This article is licensed under a Creative Commons Attribution 4.0 International License, which permits use, sharing, adaptation, distribution and reproduction in any medium or format, as long as you give appropriate credit to the original author(s) and the source, provide a link to the Creative Commons licence, and indicate if changes were made. The images or other third party material in this article are included in the article’s Creative Commons licence, unless indicated otherwise in a credit line to the material. If material is not included in the article’s Creative Commons licence and your intended use is not permitted by statutory regulation or exceeds the permitted use, you will need to obtain permission directly from the copyright holder. To view a copy of this licence, visit <http://creativecommons.org/licenses/by/4.0/>.

© The Author(s) 2020